Triple bulk heterojunctions as means for recovering the microstructure of photoactive layers in organic solar cell devices

Zhipeng Kan [a], Letizia Colella [a,b], Eleonora V. Canesi [a,*], Giovanni Lerario [a],
R. Sai Santosh Kumar [a], Valentina Bonometti [c], Patrizia. R. Mussini [c], Gabriella Cavallo [b],
Giancarlo Terraneo [a,b], Pichaya Pattanasattayavong [d], Thomas D. Anthopoulos [d],
Chiara Bertarelli [a,b], Panagiotis E. Keivanidis [a,**]

[a] Center for Nano Science and Technology@Polimi, Istituto Italiano di Tecnologia, via Pascoli 70/3, 20133 Milano, Italy
[b] Dipartimento di Chimica, Materiali e Ing. Chimica "G. Natta", Politecnico di Milano, piazza Leonardo da Vinci 32, 20133 Milano, Italy
[c] Dipartimento di Fisica Chimica ed Elettrochimica, Università degli Studi di Milano, via Golgi 19, 20133 Milano, Italy
[d] The Blackett Laboratory, Department of Physics, Imperial College London, Exhibition Road, South Kensington, London SW7 2AZ, United Kingdom

1. Introduction

During recent years significant improvements have been achieved in the power conversion efficiency (PCE) of organic photovoltaic (OPV) systems. Breakthrough PCE values, for active layers consisting of a conjugated polymer and a fullerene derivative, have risen from the early record of 2.5% [1] to the order of 10% [2–4], increasing the probability for OPV technology to gain access in commercial applications. One of the well-studied OPV composites consists of the electron-donor poly(3-hexylthiophene) (P3HT) polymer blended with the electron-acceptor phenyl-C61-butyric acid methyl ester (PCBM) fullerene derivative [5]. In addition, new formulations of next-generation materials have been disclosed in the literature [6,7].

Apart from the search of new *n*-type materials that can replace the widely used fullerene based derivatives, smart processing protocols have been also sought for the alternative development of organic photovoltaic films based on the use of ternary photo-active composites [8,9] and solvent additives [10–13]. The positive effect of using a third photoactive additive in the binary OPV composite layer on the photovoltaic efficiency of devices has been demonstrated in several recent reports. The use of ternary solid state mixtures has been suggested as a practical method for imposing control over the layer morphology of the OPV layer [14]. Another report has suggested that the use of organic binary mixtures dispersed in insulating polymeric matrices can lead to the fabrication of mechanically robust flexible OPV devices [15]. More recently, a report on the photophysical properties of hybrid ternary photoactive composites based on near-infrared absorbing PbS quantum dots has addressed the mechanism of charge photogeneration in P3HT:PCBM:QD layers [16]. Furthermore, ternary OPV films exhibited improved P3HT crystallinity. [17,18].

* Corresponding author. Tel.: +39 0223994712.
** Corresponding author. Tel.: +39 0223999806.
 E-mail addresses: eleonora.canesi@iit.it (E.V. Canesi),
pekeivan@iit.it (P.E. Keivanidis).

The use of ternary mixtures for the optimization of device properties is therefore ongoing and further analysis on the properties of devices based on these systems is required. One of the main prerequisites for a successful realization of OPV ternary systems seems to be the favourable energetic alignment for achieving a cascade-like arrangement in the frontier orbitals of the photoactive components in the composite [19–21].

In this paper we demonstrate a simultaneous improvement in the microstructure and in the photon harvesting properties of an organic photovoltaic layer by using a minimal amount, i.e. 0.3 wt% −0.6 wt%, of a third component. In particular we use a thiophene-based phenoquinone derivative, 5,5′-bis(3,5-di-*tert*-butyl-4-oxo-2,5-cyclohexadiene-1-ylidene)-5,5′-dihydro-2,2′-bithiophene (QBT) for the realization of bulk triple-heterojunction photovoltaic devices based on P3HT:PCBM:QBT ternary blend films. We investigate the effects of varying the QBT content on the performance of the P3HT:PCBM:QBT composites by using a P3HT of high regioregularity. In order to prevent losses in the open-circuit voltage of devices of these systems, caution was taken for utilizing a third QBT species with a LUMO level that is comparable to that of PCBM. With the use of QBT as the third component, our aim is two-fold, pointing both at the enhancement of the charge generation processes via the optimization of the layer microstructure and at the improvement of light harvesting strength of the modified P3HT:PCBM:QBT composite.

Based on composition dependent differential scanning calorimetry (DSC) and X-ray diffraction (XRD) experiments we show that the addition of the QBT component at low quantities improves the overall crystallinity of the P3HT matrix in the ternary layer and it results in the enlargement of the P3HT crystallites. Moreover, the use of QBT increases the fraction of the absorbed light that is used effectively for the production of photocurrent.

In a P3HT:PCBM binary blend photoexcited PCBM molecules can potentially undergo photoinduced hole-transfer to P3HT, however the efficiency of this step is expected to be limited by the large energetic gap (≈ 1 eV) between the HOMO levels of P3HT and PCBM. Previous studies on the QBT derivative have presented the occurrence of photo-induced hole transfer from QBT to a conjugated polymer with an ionization potential (IP) similar to that of P3HT, namely poly[2-methoxy-5-(2′-ethyl-hexyloxy)-1,4-phenylene vinylene] (MEH-PPV) [22]. We now extend the utilization of QBT by enabling an energy transfer step from PCBM to QBT that is followed by photo-induced hole transfer from QBT to P3HT. We thus suggest that the use of low content additives such as quinoid derivatives helps in the improvement of the device performance by utilizing the high energy photons of the absorbed light that are normally lost due to unfavourable energetic alignment in the HOMO levels of the donor and acceptor components that comprise the OPV photoactive layer. In addition, the light absorbing power of the QBT component at low photon energies in the spectral region of 700 nm enhances further the light harvesting capabilities of the P3HT:PCBM:QBT ternary system and it results in an improved photocurrent generation in devices made of the ternary layers.

Our strategy is verified by the observed 47% increase in the power conversion efficiency of ternary-based devices, in respect to the reference binary P3HT:PCBM device, and supported by spectroscopic evidences.

2. Materials and methods

2.1. Synthesis of QBT

All reactions were carried out under a dry, oxygen-free, argon atmosphere. Unless otherwise specified, all chemicals were commercial (Sigma Aldrich). Dry solvents were freshly used or maintained over molecular sieves.

2.1.1. 1-Trimethylsilyloxy-2,6-di-tert-butyl-4-bromo benzene (1)

28 ml of butyllithium 2.5 M in hexane (70.1 mmol) were dropped in a solution of 4-bromo-2,6 di-*tert*-butyl-phenol (20 g, 70.1 mmol) in dry THF (100 ml) at −78 °C. After 10 min, $(CH_3)_3$ SiCl (9.75 ml, 77.1 mmol) was added and after 15 min the mixture was slowly warmed to room temperature. After overnight stirring, H_2O was added and the reaction mixture was extracted with CH_2Cl_2 and dried over Na_2SO_4. Purification by flash chromatography on silica gel (petroleum ether: $CH_2Cl_2=9:1$) afforded the desired product **1** as a yellowish solid in 99% yield. ^{1}H NMR (400 MHz, CDCl$_3$), δ (ppm): 7.32 (s, 2H, Ph-H), 1.39 (s, 18H, t-Bu), 0.41 (s, 9H, −OSiMe$_3$).

2.1.2. Tris(3,5-bis-di-tert-butyl-4-trimethylsilyloxy phenyl)boroxin (2)

3.4 ml of butyllithium 2.5 M in hexane (8.4 mmol) were dropped in a solution of **1** (2 g, 5.6 mmol) in dry THF (20 ml) and TMEDA (4 ml) at −78 °C. After 1 hour, B(OC$_3$H$_7$)$_3$ (5.2 ml, 22.4 mmol) was added and after 45 minutes the mixture was slowly warmed to room temperature. After overnight stirring, a saturated aqueous solution of NH$_4$Cl was added. The reaction mixture was extracted with diethyl ether/H$_2$O and dried over Na$_2$SO$_4$. Purification by flash chromatography on silica gel (petroleum ether:ethyl acetate=2:1) afforded the desired product **2** as a yellowish solid in 66% yield. ^{1}H NMR (400 MHz, CDCl$_3$), δ (ppm): 8.18 (s, 6H, Ph-H), 1.49 (s, 54H, t-Bu), 0.46 (s, 27H, -OSiMe$_3$).

2.1.3. 5,5′-Bis(3,5-di-tert-butyl-4-hydroxyphenyl)-2, 2′-bithiophene (3)

Pd(PPh$_3$)$_4$ (130 mg, 0.112 mmol), tris(3,5-bis-di-tert-butyl-4-trimethylsilyloxy phenyl)boroxin (**2**) (1 g, 1.10 mmol) and K$_2$CO$_3$ aq 1 M (907 mg, 6.58 mmol in 6.5 ml H$_2$O) were added to a solution of 5,5′-dibromo-2,2′-bithiophene (239 mg, 0.736 mmol) in 13 ml of degassed DME. After refluxing overnight, the reaction mixture was extracted with diethyl ether/H$_2$O and dried over Na$_2$SO$_4$. Purification by flash chromatography on silica gel (petroleum ether:ethyl acetate=2:1) afforded 360 mg of a yellow solid (**3**), in 86% yield. ^{1}H NMR (400 MHz, CDCl$_3$), δ (ppm): 7.41 (s, 4H, Ph-H), 7.11 (*d*, 2H, Th-H, *J*=3.8 Hz), 7.08 (*d*, 2H, Th-H, *J*=3.8 Hz), 5.27 (*s*, 2H, −OH), 1.49 (*s*, 36H, t-Bu).

2.1.4. 5,5′-Bis(3,5-di-tert-butyl-4-oxo-2,5-cycloexadien-1-ylidene)-5,5′-dihydro-2,2′-bithiophene (QBT)

K$_3$Fe(CN)$_6$ (1.42 g, 4.32 mmol) and KOH 0.2 M (2.42 g, 43.2 mmol in 220 ml H$_2$O) were added to a solution of **3** (0.250 g, 0.432 mmol) in CH$_2$Cl$_2$ (150 ml). After 3 h of vigorous stirring, the mixture was extracted with CH$_2$Cl$_2$/H$_2$O and dried over Na$_2$SO$_4$. After solvent removal, the desired product (QBT) was obtained in 98% yield.[1] H-NMR (400 MHz, CDCl$_3$), δ (ppm): 7.51 (*m*, 4H, Ph-H), 7.42 (*d*, 4H, Th-H, *J*=5.14 Hz), 1.37 (*s*, 36H, t-Bu).

2.2.. Materials processing and solution preparation

Regio-regular P3HT (Mw=65,200 g mol^{-1}, *D*=2.2, RR=95.7%) was purchased from Merck, amorphous polystyrene (Mw=350,000 g mol^{-1}, *D*=2.05) was purchased from Sigma Aldrich, PCBM was purchased from Solenne BV. All materials were used as received without any additional purification. Binary films of PS:QBT, P3HT:QBT and ternary blend films of P3HT:PCBM:QBT with increasing QBT content were fabricated by dissolving the materials in chlorobenzene, followed by stirring for 30 min before spin coating. Complete solubility of QBT in chlorobenzene is achieved for all the solution

concentrations used. For the case of the ternary systems the ratio of P3HT:PCBM was kept to 1:1. Thermal annealing of the P3HT:PCBM: QBT layers was performed at 140 °C for 15 min and rapidly quenched back to room temperature.

2.3. Cyclic voltammetry

All the materials were characterized by cyclic voltammetry, CV, at potential scan rates typically ranging from 0.02 to 1.00 V s^{-1}, in 0.4 mM solutions of the CH$_2$Cl$_2$ solvent (Sigma-Aldrich, puriss. p.a.), deaerated by N$_2$ purging before each experiment. 0.1 M tetrabutylammonium perchlorate, TBAP (Fluka, puriss. electrochemical grade), was used as the supporting electrolyte, in a 4 cm^3 cell equipped with a presaturator. The ohmic potential drop was compensated by the positive feedback technique. The experiments were carried out using an Autolab PGSTAT 12 potentiostat of Eco-Chemie (Utrecht, The Netherlands), run by a PC with the GPES 4.9 software of the same manufacturer. The working electrode was a 0.071 cm^2 glassy carbon GC disk embedded in Teflon$^®$ by Amel (Milan, Italy). The counter electrode was a platinum wire. The operating reference electrode was an aqueous saturated calomel one (SCE) in a double bridge containing a CH$_2$Cl$_2$+0.1 M TBAP solution, to avoid water and KCl pollution of the working solution. All the measured potentials were then referred to the Fc$^+$/Fc couple (the intersolvental redox potential reference currently recommended by IUPAC) [23,24] by recording a CV scan of ferrocene in the working medium, immediately after the measurements in order to have the same experimental setup while avoiding possible interference between the measured molecule and the redox couple. 1 It was found that its value was fairly different from the tabulated value of −0.495 V in our CH$_2$Cl$_2$ working solution, so the measured peak potentials were referred to the values actually obtained for the Fc$^+$/Fc couple in the working conditions. The optimized finishing procedure for the working disk electrodes consisted in surface polishing with a diamond powder of 1 μm diameter of Aldrich on a wet DP-Nap cloth of Struers.

2.4. Thermal properties

5 mg of free standing films were taken from glass substrates of drop-casted as spun films of P3HT:PCBM and P3HT:PCBM:QBT and they were filled into the DSC pan. DSC thermograms for all samples were measured with DSC SEIKO 6300, under nitrogen. The DSC scans were ran in five consecutive steps: (a) from −10 °C to 140 °C, (b) from 140 °C to −10 °C, (c) from −10 °C to 320 °C, (d) from 320 °C to −10 °C and (e) from −10 °C to 500 °C. In all cases the heating and cooling rate was 10 °C min^{-1}. At the end of step (a) the samples were kept at 140 °C for 15′ prior the initiation of step (b). The enthalpy of melting (ΔH_m) and crystallization (ΔH_c) for each P3HT:PCBM;QBT composition was obtained by integrating the melting peak in the DSC heating run of step (c). TGA was measured with a SEIKO 6200.

2.5. UV–vis, time-integrated photoluminescence (PL) spectroscopy and continuous-wave photo-induced absorption (cw-PIA)

UV–vis absorption spectra of the fabricated films were recorded with a Perkin-Elmer, Lambda1050 spectrometer. Photoluminescence spectra of the fabricated films were recorded with a Horiba Jobin Yvon NanoLog spectrofluorometer or after photoexcitation of the samples with a 532 nm laser diode. For the cw-PIA measurements, excitation was provided by two laser diodes delivering 475 nm and 375 nm cw laser beam. The pump-modulation is obtained using a chopper at 228 Hz. The probe beam for the measurement was produced using a tungsten/halogen lamp. The cw-PIA signals were measured using a phase-sensitive lock-in technique with a monochromator and a Si photodiode. PL signals

were eliminated by subtracting the spectrum measured without the probe beam. All the measurements are performed in vacuum (10^{-6} mbar) to avoid any photo-oxidation of the samples.

2.6. Solar cell device fabrication and characterization

Triple-junction P3HT:PCBM:QBT solar cells were obtained by spin coating the ternary mixture onto indium tin oxide coated glass substrates, which had been oxygen plasma etched and then coated with a 50 nm layer of poly(3,4-ethylenedioxythiophene): poly(styrenesulfonate) (PEDOT:PSS). Typical active layer film thicknesses were 120–140 nm. Devices of 5.2 mm^2 area were defined by evaporation of Al metal cathodes (80 nm) through a shadow mask. For all annealed devices thermal annealing took place in a N$_2$-filled glovebox, after the deposition of the metal cathode. Glass slides of 1 mm thickness were attached onto the top metal electrode side of the devices by degassed epoxy for encapsulation. Current–voltage of the fabricated solar cells were recorded with a 2440 Keithley electrometer and a Sol3A Oriel solar simulator (AM 1.5 G) with an irradiance of 0.92 mW/cm^2. For each system characterized the reproducibility of the results was checked by measuring at least four to six devices.

2.7. X-ray diffraction

X-Ray diffraction (XRD) patterns were collected using a Bruker D8 Advance X-Ray diffractometer, operating in reflection mode with Ge-monochromated Cu Kα1 radiation (λ=1.5406 Å) and a linear position-sensitive detector; with a 2θ range 4−30°, a step size 0.016° and exposure time 1.5 s per step. Samples were mounted in Ni-coated Cu sample holder with motorized z-position. Diffraction patterns were collected at room temperature. All recorded XRD patterns were corrected for the baseline and the peak profiles were fitted with a Pearson VII functions for extracting the d spacing and peak width values. The peak position and the full-width at half maximum height (FWHM) of the peaks were obtained using QualX software [25]. The crystallite sizes were estimated based on the Scherrer equation [26]. The overall degree of crystallinity for P3HT in the ternary blend has been estimated integrating the area underneath the XRD peak at 2θ=5.3°.

2.8. Atomic force microscopy imaging

Surface topography of all ternary annealed blend films was studied by atomic force microscopy (AFM) using an Agilent 5500 in tapping mode under ambient conditions. Topography, amplitude, and phase images were recorded simultaneously.

3. Results

3.1. Materials

The chemical structure of the quinoid molecule QBT used in this study is shown in Fig. 1a together with the molecular structures of P3HT and PCBM. The synthetic route of QBT consists in a Suzuki coupling between tris(3,5-bis-di-*tert*-butyl-4-trimethylsilyloxy phenyl)boroxin and 5,5′-dibromo-2,2′-bithiophene catalyzed by tetrakis (triphenylphosphine) palladium(0). The afforded aromatic compound (5,5′-Bis(3,5-di-*tert*-butyl-4-(hydroxy)phenyl)-2,2′-bithiophene) is subsequently oxidized by K$_3$Fe(CN)$_6$ to yield the corresponding quinoid molecule [27]. In chloroform solution, the UV–vis spectrum of QBT (Fig. 1b) exhibits an intense absorption band located in the spectral region around 680 nm and shoulders at 567 nm, 618 nm and 747 nm. The high-energy shoulders have been assigned previously to the Franck–Condon vibronic structure related to the most intense
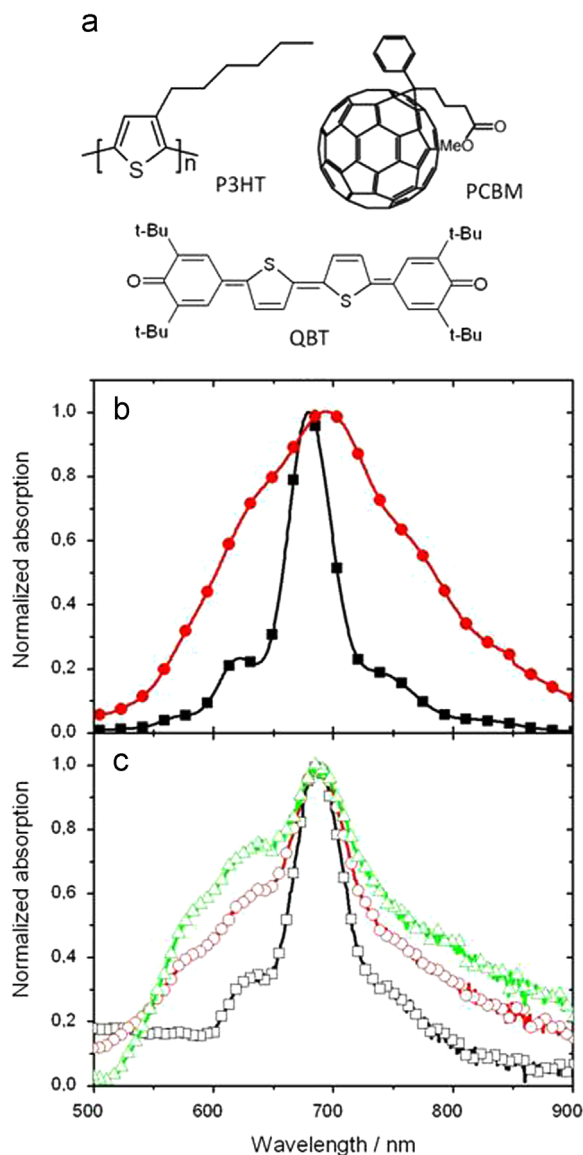
Fig. 1. Molecular structures and UV–vis characterization. (a) Molecular structure of the materials used in this study. UV–vis absorption spectra of (b) dilute ($< 10^{-5}$ M) QBT in CHCl$_3$ (filled squares) and of a QBT film spun from CHCl$_3$ solution (filled circles). (c) PS:QBT films with QBT concentration of 3 wt% (open squares), 10 wt% (open circles) and 50 wt% (open triangles). All films were spun on glass substrates.

Material	$E_{p,a}$ (Volts)	$E_{p,c}$ (Volts)	HOMO (eV)	LUMO (eV)
P3HT	0.180	–	−4.98	−2.9[21]
QBT	0.270	−0.861	−5.07	−3.94
PCBM	1.001	−0.965	−5.80	−3.84

properties in solution, by means of cyclic voltammetry (CV) versus the intersolvental potential standard of the Fc$^+$/Fc couple. Based on the first oxidation and reduction potentials E_a and E_c (Supplementary data) the energy of the highest occupied molecular orbitals (HOMO) and lowest unoccupied molecular orbitals (LUMO) were calculated according to Eqs. (1) and (2), where e corresponds to the number of exchanged electrons[29,30].

$$E_{HOMO}(eV) = -e[E_a(V \text{ vs. } Fc^+|Fc) + 4.8 \ (V \ Fc^+|Fc \text{ vs. zero})] \qquad (1)$$

$$E_{LUMO}(eV) = -e[E_c(V \text{ vs. } Fc^+|Fc) + 4.8 \ (V \ Fc^+|Fc \text{ vs. zero})] \qquad (2)$$

These equations are consistent with the absolute value for the normal hydrogen electrode (NHE) critically assessed in the review paper by Trasatti [31]. Since not all of the observed redox peaks of the three molecules exhibited electrochemical reversibility [32] we have chosen to consider the peak maxima of the recorded redox waves for calculating the energies of the HOMO and LUMO of each material. Table 1 reports the determined energy values of the HOMO levels E_{HOMO} of the studied materials which are found in good agreement with the previously reported values for P3HT and PCBM [19,21,33].

Moreover, it is shown that the energy of the LUMO for QBT $E_{LUMO,QBT} = -3.94$ eV is appropriate for considering QBT as an air-stable organic n-type semiconductor [34]. In addition we found that $E_{HOMO,QBT} = -5.07$ eV; hence $E_{HOMO,QBT}$ lies in between the $E_{HOMO,P3HT}$ and $E_{HOMO,PCBM}$ and it allows the efficient hole extraction. The E_{LUMO} value for P3HT was not measurable due to the limited available potential window of our experimental set-up.

Fig. 2 depicts a sketch of the energetics for the triple bulk heterojunction of P3HT:PCBM:QBT.

3.3. Thermal characterization

In order to address the effect of the QBT addition in the thermal properties of the ternary mixture we have recorded DSC thermograms of the P3HT:PCBM:QBT systems. The temperatures of melting (T_m) and crystallization (T_c) were taken by the maximum of peaks found in the recorded DSC thermograms. Table 2 reports the enthalpies of melting (ΔH_m) and crystallization (ΔH_c) together with the corresponding T_m and T_c temperatures of these samples as a function of the QBT content.

3.4. Structural characterization

A set of ternary composite P3HT:PCBM:QBT annealed films were prepared on glass substrates and X-ray diffraction (XRD) patterns were recorded as a function of the QBT content. Fig. 3 presents the XRD data and Table 3 reports the determined P3HT crystallite sizes for each QBT loading. The XRD peak at $2\theta = 5.3°$ was used for determining the d_{100} spacing that corresponds to the interchain distance of adjacent P3HT chains [14,35–37]. An estimation of the total crystallinity of each P3HT:PCBM:QBT sample was possible by comparing the values of the area under the XRD peak at $2\theta = 5.3°$ for each QBT loading with the corresponding value of a P3HT film that was annealed in identical conditions to those used for the P3HT:PCBM:QBT samples.

peak, whereas the low-energy shoulder has been attributed to electronic transitions due to a low lying double-exciton state [28]. In the solid state, the absorption spectrum of QBT exhibits a spectral broadening of the main absorption peak. The thermal properties of the quinoid derivative were studied by means of differential scanning calorimetry (DSC) and thermogravimentric analysis (TGA). According to TGA, QBT is thermally stable in the temperature range of 20–200 °C. Beyond 220 °C QBT degrades and TGA detects a minor weight loss at around 230 °C, while the most significant loss starts at 370 °C. The DSC and TGA results for QBT are presented in the Supplementary data. Section 3.3 below presents a detailed study of the thermal properties of the P3HT:PCBM:QBT ternary mixtures.

3.2. Electrochemistry

In order to determine the energies of the frontier molecular orbitals of P3HT, PCBM and QBT, we have investigated their redox
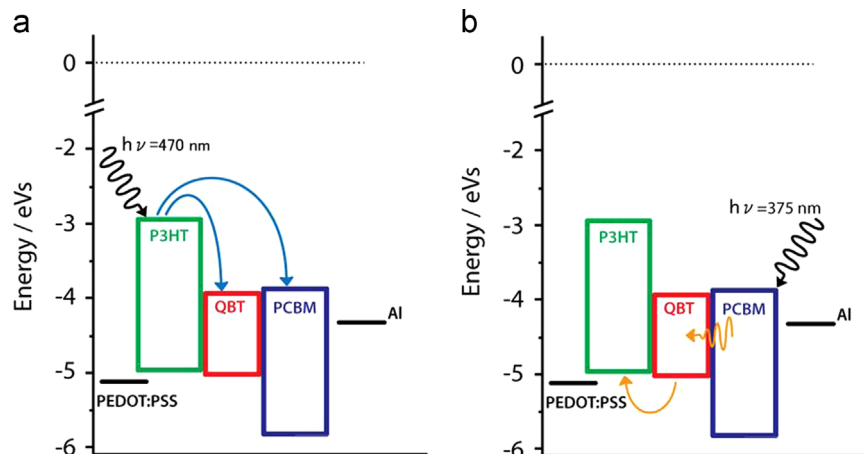
Fig. 2. Sketch of ternary blend energetics and proposed excited state pathways. Schematic representation of the energy levels of P3HT, PCBM, QBT, as obtained by cyclic voltammetry. The LUMO$_{P3HT}$ is taken as −2.9 eV. (a) Excited state pathway for charge photogeneration after photoexcitation of the P3HT component. P3HT excitons dissociate via an electron transfer step at a P3HT/QBT and P3HT/PCBM interface. (b) Excited state pathway for charge photogeneration after photoexcitation of the PCBM component. PCBM excitons energy transfer to QBT. QBT exciton then dissociate via a hole transfer step at a QBT/P3HT interface.

Table 2

Ternary blends DSC results. DSC results for the annealed P3HT:PCBM:QBT films with increasing QBT content. T_m and T_c correspond to the temperature of melting and crystallization respectively. The determined values for the enthalpy of melting (ΔH_m) and enthalpy of crystallization (ΔH_c) are also reported. In all samples the relative P3HT:PCBM mass ratio was kept at 1:1.

QBT (wt%)	T_m (°C)	ΔH_m (J/g)	T_c (°C)	ΔH_c (J/g)
0	220.0	8.89	157.4	−4.72
0.3	219.9	9.09	158.9	−4.97
0.6	220.1	9.98	156.1	−6.09
1	220.5	9.07	154.9	−4.57
3	216.7	6.52	141.3	−2.22

Table 3

Ternary blends XRD results. XRD results for the annealed P3HT:PCBM:QBT films with increasing QBT content. 2θ is the position of the d$_{100}$ peak, α is the deduced interchain distance, FWHM is the full width at half maximum of the d$_{100}$ peak, D is the determined P3HT crystallite size, A is the integrated area of the d$_{100}$ peak. For an annealed P3HT film of 70 nm, $D=31,1$ nm and $A=265.5$. All films were deposited on glass substrates by spin-coating.

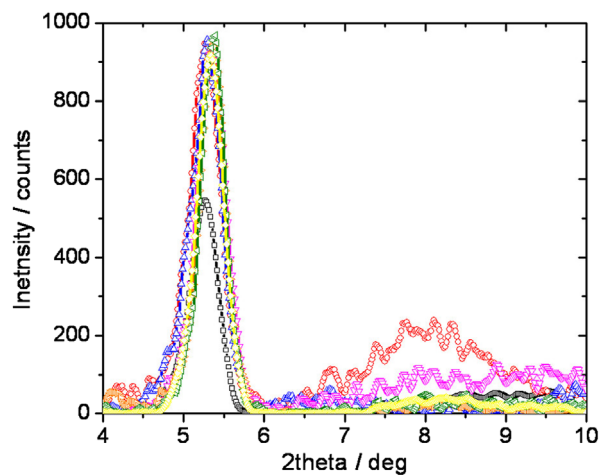| QBT (wt%)	2θ (deg)	α (Å)	FWHM d100 (deg)	D (nm)	A (cps deg)
0	5.272	16.8	0.320	24.9	123.9
0.3	5.295	16.7	0.288	27.6	230.6
0.6	5.295	16.7	0.272	29.3	232.8
1	5.343	16.5	0.320	24.9	214.7
3	5.359	16.5	0.336	23.7	199.9
6	5.392	16.4	0.320	24.9	190.5
10	5.327	16.6	0.320	24.9	198.1

Fig. 3. Ternary blends XRD patterns. XRD patterns for an annealed P3HT film and for annealed P3HT:PCBM:QBT films with QBT content of 0 wt% (squares), 0.3 wt% (circles), 0.6wt% (up triangles), 1wt% (down triangles), 3 wt% (right-tilt triangles), 6 wt% (left-tilt triangles) and 10 wt% (diamonds). In all cases the films were deposited on glass and for the ternary P3HT:PCBM:QBT samples the P3HT:PCBM mass ratio was kept at 1:1.

Fig. 4. Ternary blends UV–vis characterization. Normalized absorption spectra of P3HT:PCBM:QBT blend films on glass, with different amount of QBT in the ternary composite: 0 wt% (squares), 0.3 wt% (circles), 0.6 wt% (up triangles), 1 wt% (down triangles), 3 wt% (right-tilt triangles), 6 wt% (left-tilt triangles) and 10 wt% (diamonds). In all samples the relative P3HT:PCBM mass ratio was kept at 1:1.

Table 3 summarizes the extracted values of interchain distance and crystallite size of the studied P3HT:PCBM:QBT films. It can be seen that the addition of the QBT component is not affecting significantly the P3HT interchain distances suggesting that the unit cell of P3HT in the ternary systems remains unaltered. However, by adding 0.3–0.6 wt% QBT the P3HT crystallite size increases by 15%
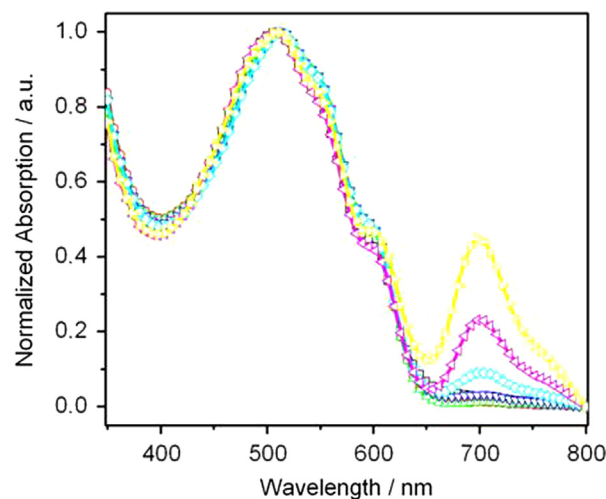
and the overall crystallinity of the ternary films increases. Particularly for the case of the ternary sample with 3 wt% QBT content the overall crystallinity of the film is found improved in respect to the binary

P3HT:PCBM film, in contrast with the ΔH_m and ΔH_c values of these system that were lower than the binary P3HT:PCBM composite (Table 2). We assign this discrepancy to different conditions of the measured samples that have most likely affected the fraction of the well-ordered P3HT chains in the sample: DSC thermograms were recorded for annealed thick free standing films after drop-casting whereas XRD patterns were recorded for annealed thin films of 110–130 nm thickness as prepared by spin coating.

3.5. UV–vis spectroscopy

We have measured the UV–vis spectra of QBT binary composite films by using polystyrene (PS) as an optically inert binder for a series of PS:QBT ratios (Fig. 1c). At high QBT contents clear changes can be observed in the relative intensities of the low- and high-energy shoulders together with a spectral broadening of the main band. For the 50 wt% content of QBT the absorption of PS:QBT resembles to that of a pure QBT film (Fig. 1b).

Fig. 4 presents the UV–vis absorption spectra of the ternary annealed P3HT:PCBM:QBT blend films with increasing QBT content. In these samples the relative ratio of P3HT:PCBM was kept as 1:1 and the QBT content was varied between 0 wt% and 10 wt% in respect to the total mass content of the ternary mixture. For these systems no variations were found in the thickness of the P3HT: PCBM:QBT films in respect to the binary P3HT:PCBM film. The film thickness of all P3HT:PCBM:QBT films and the non-normalized UV–vis data can be found in the Supplementary data.

3.6. PL and cw-PIA spectroscopy

In order to study how the addition of the quinoid component affects the quenching efficiency of the P3HT excitons in the P3HT: PCBM:QBT triple junctions we have performed time-integrated photoluminescence (PL) experiments in the P3HT:PCBM:QBT blend films. Annealed P3HT:PCBM:QBT films with increasing QBT content were photoexcited at 532 nm (where P3HT mainly absorbs) and the spectral integral of the P3HT PL signal was compared with the corresponding spectral integral of an annealed P3HT:PCBM film. Based on this comparison we have determined the quenching efficiency of P3HT emission that can be assigned to the presence of the QBT in the ternary system. Fig. 5a presents the QBT-composition dependent quenching efficiency of the P3HT PL emission in the annealed P3HT:PCBM:QBT films. The PL quenching efficiency is gradually increasing as the QBT content increases and it reaches a maximum value of 97% when the QBT loading is 6 wt%.

Secondary PL quenching experiments in ternary blends of PS: P3HT:QBT were performed with variable QBT content. In these samples the relative ratio of PS:P3HT was kept as 1:4 and the QBT content was varied between 0 wt% and 10 wt% in respect to the total mass content of the ternary mixture. After photoexcitation of the PS:P3HT:QBT at 530 nm it was found that the P3HT excitons are quenched by 70 wt% in the presence of 3 wt% of QBT. The PL spectra of the annealed P3HT:PCBM:QBT and PS:P3HT:QBT films can be found in the Supplementary data.

In order to quantify the charge photogeneration yield in the ternary P3HT:PCBM:QBT composites we have performed composition dependent continuous-wave (cw) photo-induced absorption (PIA) experiments on P3HT:PCBM:QBT films. The PIA signal of the cw-PIA measurement is an appropriate indicator for evaluating the concentration of long-lived species such as triplet and polaron states. In our cw-PIA experiment we have monitored the spectral region of 1000 nm where the P3HT cation absorbs [38]. The absorption cross-section of the P3HT cation is an order of magnitude larger than the corresponding absorption cross-section of PCBM anion at that wavelength [39]. In addition, the reduced form of QBT does not exhibit any absorption at the spectral range of 1000 nm [40]. For the
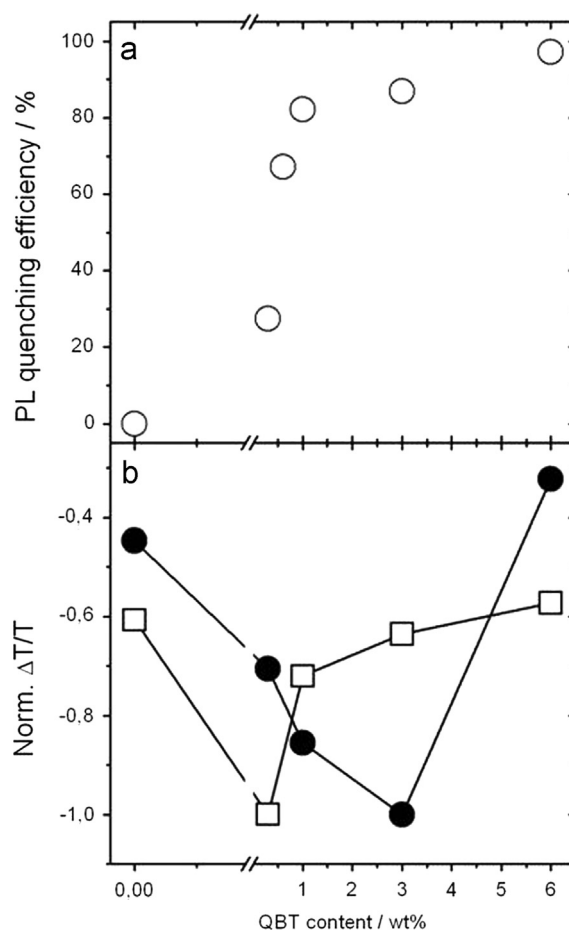

Fig. 5. Ternary blends photoluminescence and cw-PIA characterization. (a) The % quenching efficiency of the P3HT luminescence as a function of the QBT content in ternary blends of P3HT:PCBM:QBT on glass. Excitation was at 532 nm. (b) QBT composition dependence of the normalized cw-PIA absorption of the P3HT polaron at 1000 nm in ternary blends of P3HT:PCBM:QBT on glass. Photoexcitation was at 470 nm (open squares) and at 375 nm (filled circles).

photoexcitation of the blends two different wavelengths were chosen in order to address the effect of selectively exciting each of the blend components. In particular we have photoexcited the P3HT:PCBM:QBT blend films at 470 nm, where P3HT mainly absorbs, and at 375 nm, where PCBM mainly absorbs. Fig. 5b presents the composition dependent cw-PIA results for these two wavelengths, normalized to the maximum PIA value for each of the two measurements. For both wavelengths the photoexcitation intensity was kept in the level of 12.5 mW cm^{-2} and no differences were observed in the composition dependent trend of the 470 nm excitation when the intensity was raised to 41 mW cm^{-2}. For the direct photoexcitation of P3HT at 470 nm, the maximum PIA signal is observed at the QBT content of 0.3 wt% whereas for the direct photoexcitation of PCBM at 375 nm the optimum QBT content shifts to 3 wt%. The cw-PIA spectra of the PH3T:PCBM:QBT with increasing QBT content for both excitation wavelengths are shown in the Supplementary data.

3.7. Solar cells characterization

We have fabricated annealed devices of P3HT:PCBM:QBT ternary blends with increasing QBT content. Fig. 6 presents the composition dependent EQE spectra of the ternary systems together with the corresponding J–V curves obtained under simulated solar illumination (0.92 Suns, AM1.5G). In respect to the annealed binary P3HT:PCBM system, the performance of the P3HT:PCBM:QBT system is greatly improved when the QBT
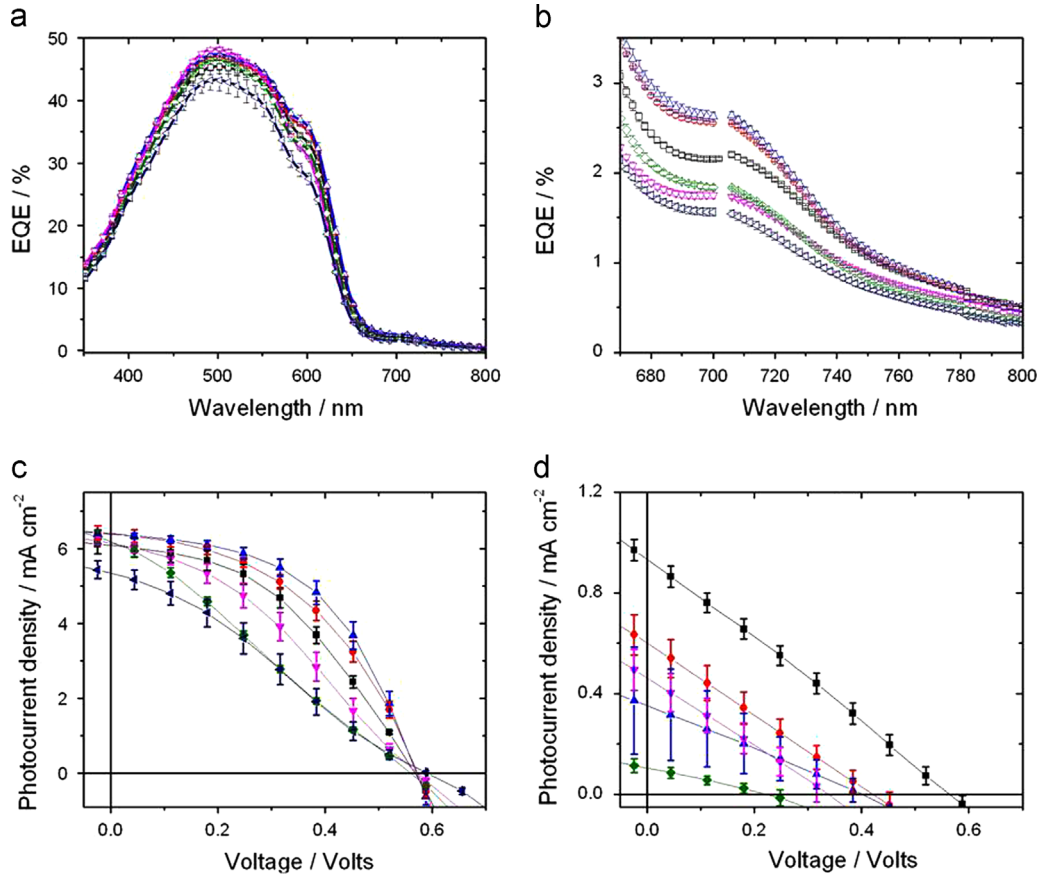
Fig. 6. Ternary blends photovoltaic EQE spectra and J-V characteristics. (a) Composition dependent EQE spectra of devices made of annealed P3HT:PCBM:QBT photoactive layers with increasing QBT content, (b) magnification of the EQE spectra presented in (a) with emphasis in the spectral region of 670 nm–800 nm, (c) J–V characteristics obtained under simulated solar illumination (0.92 Suns, AM1.5G) for devices made of (c) annealed and (d) as-spun P3HT:PCBM:QBT photoactive layers with increasing QBT content. 0 wt% (squares), 0.3 wt% (circles), 0,6 wt% (up triangles), 1 wt% (down triangles), 3 wt% (stars) and 6 wt% (left triangles). In all samples the relative P3HT:PCBM mass ratio was kept at 1:1.

Table 4
Ternary blends device metrics. QBT composition dependence of the main device metrics of the annealed P3HT:PCBM:QBT solar cells.

QBT (wt%)	Voc (Volts)	Jsc (mA cm^{-2})	FF (%)	PCE (%)
0	0.577 ± 0.009	6.306 ± 0.236	39.8 ± 0.4	1.558 ± 0.076
0.3	0.572 ± 0.005	6.690 ± 0.156	40.5 ± 0.9	1.669 ± 0.059
0.6	0.568 ± 0.005	6.897 ± 0.260	54.3 ± 1.4	2.287 ± 0.076
1	0.569 ± 0.005	6.245 ± 0.196	51.8 ± 1.3	1.981 ± 0.080
3	0.574 ± 0.006	5.341 ± 0.281	24.2 ± 1.2	0.798 ± 0.060
6	0.591 ± 0.003	4.565 ± 0.034	23.1 ± 0.9	0.669 ± 0.025

content is in the range of 0.3–0.6 wt%. In comparison with the binary device (0 wt% QBT), the annealed ternary device with QBT content of 0.6 wt% exhibits an improvement of the EQE at the wavelength of 500 nm, where the maximum photocurrent of the two devices is detected ($EQE_{500 nm, 0 wt\%} = 45.4\%$ $\pm 1.1\%$ and $EQE_{500 nm, 0.6 wt\%} = 47.4\% \pm 0.1\%$). Moreover the addition of small amounts of QBT results in an increase in the photocurrent generation both at the high and the low photon energy parts of the spectrum. For the QBT content of 0.6 wt%, the spectrally integrated EQE in the region of 350–450 nm is found enhanced by 6.7%, whereas for the spectral region of 690–700 nm the enhancement of the spectrally integrated EQE is 22.6% (see Supplementary data for spectrally integrated EQE values). Fig. 6b depicts the improvement of the EQE spectra in the low photon energy region of 670 nm–800 nm.

In a similar fashion the J–V characteristics (Fig. 6c) of the ternary-based devices are significantly improved upon the addition of the QBT derivative. Table 4 reports the values of the open-circuit voltage (V_{oc}), short-circuit photocurrent (J_{sc}), fill factor (FF) and power conversion efficiency (% PCE) of these devices. For the QBT content of 0.6 wt% the PCE value of the ternary system is found improved by 47% mainly due to the improvement in the values of the parameters of J_{sc} and FF. These results have been obtained with a simple cell structure comprised of ITO/PEDOT:PSS/blend/Al layers: more complex structures (i.e. with the addition of blocking layers) are expected to give improved overall efficiency. However, since the beneficial role of QBT in enhancing performance of non-optimized microstructure of the active layer turns out to be an added value in the production scaling-up, the fabrication and study of optimized cell structure has not been herein considered.

In contrast to the devices made of annealed ternary layers, no improvement was found in device performance of the as-spun P3HT:PCBM devices after the addition of QBT. As Fig. 6d shows, the J–V curves of the as-spun P3HT:PCBM:QBT devices exhibit inferior electrical properties in comparison to the corresponding properties of the as-spun binary P3HT:PCBM device (see Supplementary data for EQE and J–V device metrics of as-spun samples).

3.8. Surface topography

We have performed atomic force microscopy imaging on a set of annealed P3HT:PCBM:QBT blend films on glass/ITO/PEDOT:PSS substrates, with increasing QBT content. AFM scans were performed
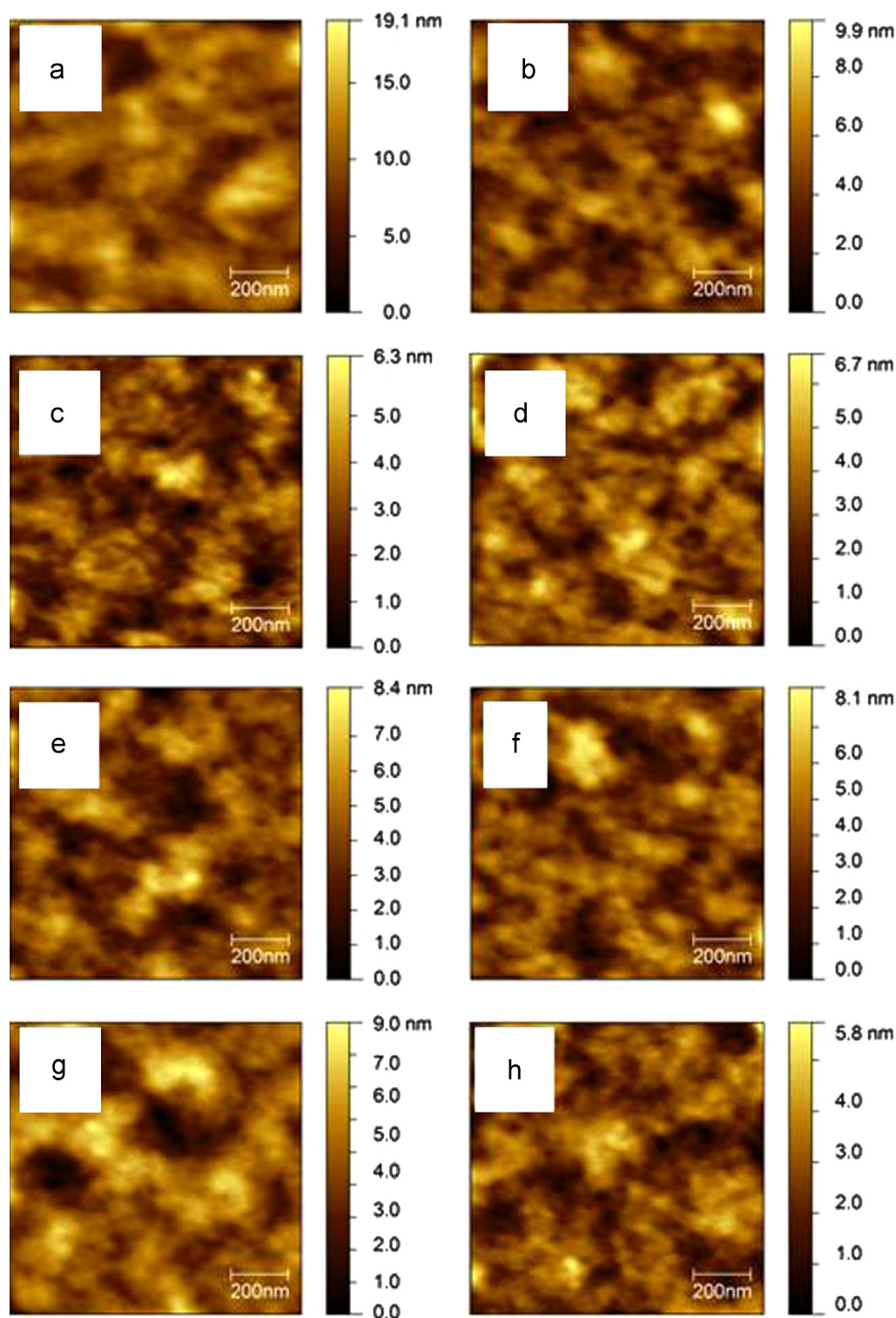
Fig. 7. Ternary blends AFM characterization. Tapping mode AFM images (1 µm scan length) for a set of annealed P3HT and P3HT:PCBM:QBT films. (a) P3HT, (b) P3HT:PCBM:QBT 0 wt%, (c) P3HT:PCBM:QBT 0.3 wt%, (d) P3HT:PCBM:QBT 0.6 wt%, (e) P3HT:PCBM:QBT 1 wt%, (f) P3HT:PCBM:QBT 3 wt% (g) P3HT:PCBM:QBT 6 wt%, (h) P3HT:PCBM:QBT 10 wt%. All samples were deposited on glass/ITO/PEDOT:PSS substrates.

in 1 µm and in 5 µm scan lengths. Due to the relative smoothness of the films, the acquisition of AFM images on smaller scan areas was not possible as the noise in the measurement was significant and the collected images were blurred. Regarding the 5 µm scan length AFM images, the annealed P3HT:PCBM film was found to have a lower root-mean-square roughness than the ternary layers with QBT content below 1 wt%. However it was difficult to visualize any changes in the surface topography of the films. Fig. 7 presents the 1

µm scan length AFM images of the studied P3HT:PCBM:QBT samples.

4. Discussion

The use of the QBT derivative as a third component in the P3HT:PCBM:QBT ternary system results in the improvement of the

PCE parameter by almost 50%. The positive impact of the QBT addition in the electrical properties of the ternary devices is reflected on the increased values of device photocurrent and fill factor (Table 4). The improvement is found after the addition of a small QBT amount (0.3–0.6 wt%) in the P3HT:PCBM:QBT layer and it is a consequence of (i) the optimization in the layer microstructure and (ii) the efficient utilization of the light that the layer absorbs.

The DSC and XRD data demonstrate that the use of QBT results in an increase in the number of well-ordered P3HT chains present in the annealed ternary layers. Higher values of ΔH_m and ΔH_c were obtained for these ternary mixtures that exhibited higher crystallinity. Moreover the use of QBT leads to an increase of the P3HT crystallite size by 9–15% (Table 3). The changes that QBT imposes in the structure of the P3HT:PCBM:QBT layer are different from those reported previously for other ternary composites of the P3HT:PCBM system. Although that a higher crystallinity was found in ternary mixtures of regio-random (RRa) and regio-regular (RR) P3HT with PCBM, the size of the P3HT crystallites was found reduced [14]. More recent results demonstrated that the addition of an amorphous polymer in the binary composite of P3HT:PCBM did not affect the crystallinity of P3HT but it resulted in the reduction of the PCBM crystallinity [41]. In both cases the content of third component in those systems was much greater than the one used for QBT in the P3HT:PCBM:QBT ternaries. For the P3HT:PCBM:QBT ternary blends we suggest that QBT functions as nucleation agent that assists the crystallization of P3HT during the cooling of the layer to RT after annealing. This is confirmed by the formation of the large P3HT crystallites that are formed at the low QBT content of 0.3-0.6% wt%. This type of heterogeneous nucleation of P3HT is assisted by QBT molecules that serve as scaffolds for the growth of the P3HT crystallites.

Based on the energetic of P3HT and QBT the dissociation of P3HT excitons is energetically favourable process. The quenching of the P3HT PL intensity that is seen in the PS:P3HT:QBT systems (Fig. S07 in Supplementary data) together with the CV results (Table 1) confirm the electronic coupling of the photoexcited P3HT with the QBT component. Taking into account that the $E_{LUMO,\ P3HT=} -2.9$ eV [21] we can assume that an efficient electron transfer reaction is expected to take place at the P3HT/QBT interfaces.

Moreover, the addition of QBT results in the structural modification of the P3HT:PCBM:QBT ternary layers. As an overall result, the presence of QBT improves the dissociation efficiency of the P3HT excitons and the charge separation efficiency of the resulting electron–hole pairs. This manifests in the increased PL quenching efficiency (Fig. 5a) and in the increased cw-PIA signal (Fig. 5b) of the long-lived P3HT polarons in the ternary P3HT:PCBM:QBT systems. Previous PL quenching studies of the annealed binary P3HT:PCBM system have reported a maximum PL quenching efficiency of $\sim 60\%$ [42]. For the P3HT:PCBM:QBT ternary systems, the quenching of the P3HT excitons is almost complete indicating a maximized generation efficiency of electron–hole pairs in the ternary blends. We assign the additional quenching of the P3HT excitons to the enhanced exciton dissociation at the P3HT/QBT interfaces in the ternary layers (Fig. 2a).

Despite the continuous increase of the P3HT exciton dissociation efficiency with increasing QBT content, the composition dependent cw-PIA data of the P3HT:PCBM:QBT films shows that the survival probability of long-lived photogeneration charges does not scale with the QBT content at high QBT loadings. For excitation at 470 nm of the ternary systems the maximum free charge generation yield is found at the QBT concentration of 0.3 wt %. Based on the XRD results (Table 3) we can suggest that free charge generation is favoured upon the enlargement of the P3HT crystallite sizes up to the value of 27–29 nm[42]. At QBT contents

higher than 0.6 wt% the P3HT crystallite size is again reduced and charge recombination prevails.

In comparison with the binary P3HT:PCBM device, the ternary device with 0.6 wt% QBT exhibits an improved EQE value at the wavelength of 500 nm (EQE_{500nm}). The effect is further enhanced for QBT loading of 1 wt% indicating that, regardless the onset of charge recombination, efficient charge transport and extraction take place in the device. For QBT loadings higher than 1 wt% the EQE_{500nm} values are found significantly reduced, albeit still higher than the corresponding value for the binary system of P3HT:PCBM.

Similarly, the increased value of FF for the QBT content of 0.3–0.6 wt% (Table 4) are attributed to the increased fraction of the crystalline volume in the P3HT:PCBM:QBT layers and to the optimal size of the P3HT crystallites that preserve the connectivity of the P3HT phase. Previous charge transport studies on ternary mixtures have shown a reduction in the carrier mobility upon the addition of a third component[14,41]. For the P3HT:PCBM:QBT system the impact of QBT addition on the charge transport properties of the layer will be discussed elsewhere.

The excessive addition of QBT beyond 0.6 wt% in the P3HT:PCBM:QBT ternaries has a detrimental effect in the charge photogeneration efficiency and in the electrical properties of the devices. The strong reduction in the FF value suggests an inefficient collection of photogenerated charges. This may be a result of an unfavourable layer microstructure in the layers with QBT content higher than 0.6 wt%. According to the acquired AFM images (Fig. 7) the addition of QBT does not modify drastically the surface topography of the P3HT:PCBM system. It is plausible that high QBT loadings can favour the mixing of the PCBM component and P3HT matrix and may reduce the crystallinity of PCBM in the bulk of the ternary layers[41]. No melting transition of the PCBM component could be detected in the DSC thermograms of the P3HT:QBT:PCBM systems indicating a low crystalline content of PCBM. We were also unable to detect a melting transition at 280 °C in the DSC thermogram of the binary P3HT:PCBM system and this further suggests that in the studied systems the PCBM component is not well segregated but it is intermixed with the P3HT matrix leading to a non-optimized P3HT:PCBM layer morphology.

Interestingly, an improvement in the cw-PIA signal of the P3HT polarons is found when the PCBM component of the ternary films is selectively photoexcited at 375 nm. Fig. 5b shows that the concentration of the P3HT polaron increases with the addition of the QBT derivative up to the QBT content of 3 wt%. The EQE data of the ternary devices also show an improvement in the photocurrent generation efficiency at the spectral region of 350–450 nm (Fig. 6a). The positive effect in EQE is maximized for the QBT content of 0.6–1 wt% (Fig. S12a in Supplementary data).

Based on these findings we suggest that after photoexcitation at high photon energies, charge photogeneration proceeds via (i) an energy transfer step from photoexcited PCBM to QBT and (ii) a photo-induced hole transfer reaction between QBT and P3HT (Fig. 2b). The spectral overlap of PCBM emission [43] with the QBT absorption (Fig. 1) further supports our hypothesis for an energy transfer step from PCBM to QBT. We have performed control experiments on PS:PCBM:QBT films for directly monitoring the PL quenching of PCBM [43] but we cannot detect any PCBM PL signal even in the absence of QBT in the films. Finally, due to the fact that photoexcited QBT is not emissive it was not possible to directly monitor the photo-induced hole transfer step from QBT to P3HT by monitoring the QBT PL quenching. However, we have verified that in the presence of QBT the luminescence of photoexcited P3HT is efficiently quenched.

For photoexcitation of the ternary films at the spectral region where the PCBM component mainly absorbs, the optimum QBT concentration for maximum P3HT polaron photogeneration (Fig. 5b) is 3 wt% whereas maximum photocurrent generation (Fig. 6a and Fig. S12b in Supplementary data) is 1 wt%. This

discrepancy suggests that although after photoexciting PCBM the maximum concentration of P3HT polarons is formed at relatively high QBT content, efficient transport and extraction of the charges takes place at relatively lower QBT content, where the layer microstructure is optimized for assisting the percolation of the charges towards the device electrodes.

The addition of the QBT derivative enhances the light absorbing power of the P3HT:PCBM:QBT system at 700 nm and an increase can be seen in the photocurrent generation of the corresponding devices in the spectral region of 690 nm–700 nm. Fig. 6b and Fig. S12c in Supplementary data show that the devices of the ternary P3HT:PCBM:QBT system with QBT content of 0.6 wt% exhibit more than 20% increase in the EQE in respect to the binary P3HT:PCBM cells. Based on the UV–vis spectra of the QBT derivative (Fig. 1b) it can be seen that the absorption band of QBT complements the absorption band of the P3HT:PCBM blend. In dilute chloroform solution ($< 10^{-5}$ M) QBT exhibits a strong absorption in the spectral region of 700 nm and the molecular absorption coefficient is $\varepsilon_{700\,nm} > 10^5\,M^{-1}\,cm^{-1}$[40]. In the solid state, for the annealed PS:QBT film with QBT loading of 0.6 wt% the attenuation coefficient at 685 nm is found $\alpha_{PS:QBT} = 4300\,cm^{-1}$ (see Supplementary data). Therefore, the triple junction of P3HT:PCBM:QBT offers the possibility for extending the light harvesting properties of the P3HT:PCBM system [21,44] at low photon energies in the region of 700 nm, where P3HT and PCBM do not absorb strongly. At high QBT content, the positive effect of extended absorption is counterbalanced by the onset of QBT aggregation that results in the deterioration of the layer microstructure and of the electrical properties of the corresponding devices. From the UV–vis spectra of the PS:QBT films it is found that at high QBT loadings QBT forms aggregates and it is conceivable that in the case of the P3HT:PCBM:QBT films the aggregation of QBT will lead to the phase separation of QBT from the P3HT matrix.

5. Conclusions

In conclusion, all-organic triple bulk heterojunctions of P3HT and PCBM, with a cascade type of HOMO levels were studied based on the use of the QBT quinoid derivative. The photoactive layers of the triple junction P3HT:PCBM:QBT with increasing QBT content were investigated in terms of electrochemical, thermal, structural, spectroscopic, electrical and morphological properties. The use of 0.6 wt% QBT as the third component has lead to a 47% increase in the power conversion efficiency of non-optimized P3HT:PCBM devices, with photoactive layers of low crystallinePCBM. The non-optimized microstructure of the reference binary P3HT:PCBM device is attributed to the low crystalline content of PCBM, as inferred by the absence of the melting transition of the PCBM component in the DSC thermograms, and to the non-ideal P3HT texture. The improvement in device performance of the triple heterojunction is the simultaneous result of (a) the optimized microstructure of P3HT in the layer and (b) the increased photon harvesting from the layer both at low and high energy parts of the solar spectrum in the presence of QBT.

The addition of 0.3–0.6 wt% QBT improves significantly the overall crystallinity of the P3HT:PCBM:QBT films and it results in an increase of the P3HT crystallite size by 15%. The increase of the P3HT domains does not have a negative influence on the P3HT exciton dissociation efficiency and it favours the generation of long-live free P3HT polarons, as evidenced by the enhanced PL quenching and the increased cw-PIA signal at 1000 nm. In respect to device metrics the improved microstructure of the ternary layers leads to improved FF and J_{SC} values. For QBT contents exceeding the optimum 0.6 wt%, QBT strongly aggregates and the P3HT crystallites become smaller. As a result of this structural deterioration in the photoactive layer, the electrical properties of the corresponding solar cells are degrading.

We propose that in the P3HT:PCBM:QBT systems charge generation proceeds via three different excited state pathways that are consistent with the relative position of energy levels of the materials involved. The direct excitation of the P3HT component results in charge generation that is driven by electron transfer between the photoexcited P3HT and both of the electron acceptors QBT and PCBM in the triple junction. Secondly, the direct excitation of PCBM causes energy transfer from the photoexcited PCBM to QBT followed by a hole transfer from QBT to P3HT. Finally, the direct excitation of QBT in the spectral region of 700 nm results in photocurrent generation via a photo-induced hole transfer from QBT to P3HT. The positive impact of these three excited state pathways on the production of photo-current is confirmed by the EQE spectra of the ternary devices that show improved EQE values at the corresponding wavelength regions.

The opportunity to recover PCE performance in OPV layers with non-optimized microstructure is of great importance in view of large scale devices production, where less control is feasible with respect to lab-scale production.

Moreover, our findings offer general guidelines for the design of future functional additives with appropriate energetics and chemical structure that can lead to the realization of the next generation ternary polymer:fullerene solar cells. The photon energy that is harvested by the fullerene component of OPV layers and which is usually lost, can be efficiently employed for the production of photocurrent if the photoactive layer is enriched by light-absorbing additives with an optical gap (E_g) smaller than the E_g of PCBM, an electron affinity (EA) comparable to the EA of PCBM, and an IP placed between the IPs of the polymer donor and the PCBM. As such, the additive can accept the energy of the photo-excited fullerene and it can additionally harvest lower energy photons that are not absorbed either by the polymer or by the fullerene. Apart from the efficient light harvesting management, additives with specifically designed molecular structures can serve as nucleation seeds for improving the microstructure of the OPV layers. Chemical structures of the additives are sought that can be used as scaffolds on which the crystallite growth of the polymer matrix can take place during the cooling phase after the thermal annealing of the OPV layer. Further studies on the influence of next generation quinoidal-based additives, with modified chemical structure, on the device performance of OPVs are required. Such a study will provide additional insights in the challenge of designing an ideal molecular additive that meets the energetic and the morphology-related requirements for efficient triple bulk heterojunction OPV composites.

Appendix A. Supporting information

- Supplementary data associated with this article can be found in the online version.

References

[1] S.E. Shaheen, C.J. Brabec, N.S. Sariciftci, F. Padinger, T. Fromherz, J.C. Hummelen, 2.5% Efficient organic plastic solar cells, Applied Physics Letters 78 (2001) 841–843.

[2] M. Helgesen, R. Sondergaard, F.C. Krebs, Advanced materials and processes for polymer solar cell devices, Journal of Materials Chemistry 20 (2010) 36–60.

[3] J. Nelson, Polymer:fullerene bulk heterojunction solar cells, Materials Today 14 (2011) 462–470.

[4] G. Li, R. Zhu, Y. Yang, Polymer solar cells, Nature Photonics 6 (2012) 153–161.

[5] M.T. Dang, L. Hirsch, G. Wantz, P3HT:PCBM, best seller in polymer photovoltaic research, Advanced Materials 23 (2011) 3597–3602.

[6] P.-L.T. Boudreault, A. Najari, M. Leclerc, Processable low-bandgap polymers for photovoltaic applications, Chemistry of Materials 23 (2011) 456–469.

[7] C.L. Chochos, S.A. Choulis, How the structural deviations on the backbone of conjugated polymers influence their optoelectronic properties and photovoltaic performance, Progress in Polymer Science 36 (2011) 1326–1414.

[8] Y.-C. Chen, C.-Y. Hsu, R.Y.-Y. Lin, K.-C. Ho, J.T. Lin, Materials for the active layer of organic photovoltaics: ternary solar cell approach, ChemSusChem 6 (2013) 20–35.

[9] T. Ameri, P. Khoram, J. Min, C.J. Brabec, Organic ternary solar cells: a review, Advanced Materials 25 (2013) 4245–4266.

[10] J. Peet, J.Y. Kim, N.E. Coates, W.L. Ma, D. Moses, A.J. Heeger, G.C. Bazan, Efficiency enhancement in low-bandgap polymer solar cells by processing with alkane dithiols, Nature Materials 6 (2007) 497–500.

[11] I.-W. Hwang, S. Cho, J.Y. Kim, K. Lee, N.E. Coates, D. Moses, A.J. Heeger, Carrier generation and transport in bulk heterojunction films processed with 1,8-octanedithiol as a processing additive, Journal of Applied Physics 104 (2008) 033706-1–033706-9.

[12] S.J. Lou, J.M. Szarko, T. Xu, L. Yu, T.J. Marks, L.X. Chen, Effects of additives on the morphology of solution phase aggregates formed by active layer components of high-efficiency organic solar cells, Journal of the American Chemical Society 133 (2011) 20661–20663.

[13] S. Chambon, R. Mens, K. Vandewal, E. Clodic, M. Scharber, L. Lutsen, J. Gelan, J. Manca, D. Vanderzande, P. Adriaensens, Influence of octanedithiol on the nanomorphology of PCPDTBT:PCBM blends studied by solid-state NMR, Solar Energy Materials and Solar Cells 96 (2012) 210–217.

[14] M. Campoy-Quiles, Y. Kanai, A. El-Basaty, H. Sakai, H. Murata, Ternary mixing: a simple method to tailor the morphology of organic solar cells, Organic Electronics 10 (2009) 1120–1132.

[15] T.A.M. Ferenczi, C. Müller, D.D.C. Bradley, P. Smith, J. Nelson, N. Stingelin, Organic semiconductor:insulator polymer ternary blends for photovoltaics, Advanced Materials 23 (2011) 4093–4097.

[16] G. Itskos, A. Othonos, T. Rauch, S.F. Tedde, O. Hayden, M.V. Kovalenko, W. Heiss, S.A. Choulis, Optical properties of organic semiconductor blends with near-infrared quantum-dot sensitizers for light harvesting applications, Advanced Energy Materials 1 (2011) 802–812.

[17] E. Lim, S. Lee, K.K. Lee, Improved photovoltaic performance of P3HT:PCBM cells by addition of a low band-gap oligomer, Chemical Communications 47 (2011) 914–916.

[18] S. Jeong, Y. Kwon, B.-D. Choi, G. Kwak, Y.S. Han, Effects of nematic liquid crystal additives on the performance of polymer solar cells, Macromolecular Chemistry and Physics 211 (2010) 2474–2479.

[19] J. Peet, A.B. Tamayo, X.-D. Dang, J.H. Seo, T.-Q. Nguyen, Small molecule sensitizers for near-infrared absorption in polymer bulk heterojunction solar cells, Applied Physics Letters 93 (2008) 163306-1–163306-3.

[20] S.S. Sharma, G.D. Sharma, J.A. Mikroyannidis, Improved power conversion efficiency of bulk heterojunction poly(3-hexylthiophene):PCBM photovoltaic devices using small molecule additive, Solar Energy Materials and Solar Cells 95 (2011) 1219–1223.

[21] M. Koppe, H.-J. Egelhaaf, G. Dennler, M.C. Scharber, C.J. Brabec, P. Schilinsky, C.N. Hoth, Near IR Sensitization of organic bulk heterojunction solar cells: towards optimization of the spectral response of organic solar cells, Advanced Function Materials 20 (2010) 338–346.

[22] T. Agostinelli, M. Caironi, D. Natali, M. Sampietro, G. Dassa, E.V. Canesi, C. Bertarelli, G. Zerbi, J. Cabanillas-Gonzalez, S.D. Silvestri, G. Lanzani, A planar organic near infrared light detector based on bulk heterojunction of a heteroquaterphenoquinone and poly[2-methoxy-5-(2[sup [prime]]-ethyl-hexyloxy)-1, 4-phenylene vinylene], Journal of Applied Physics 104 (2008) 114508-1–114508-5.

[23] G. Gritzner, J. Kuta, Recommendations on reporting electrode potentials in nonaqueous solvents, Pure and Applied Chemistry 56 (1984) 461–466.

[24] G. Gritzner, Polarographic half-wave potentials of cations in nonaqueous solvents, Pure and Applied Chemistry 62 (1990) 1839–1858.

[25] A. Altomare, C. Cuocci, C. Giacovazzo, A. Moliterni, R. Rizzi, QUALX: a computer program for qualitative analysis using powder diffraction data, Journal of Applied Crystallography 41 (2008) 815–817.

[26] P. Scherrer, Bestimmung der größe und der inneren struktur von kolloidteilchen mittels röntgenstrahlen, Nachrichten von der Gesellschaft der Wissenschaften zu Göttingen, Mathematisch-Physikalische Klasse 2 2 (1918) 98–100.

[27] D. Fazzi, E.V. Canesi, F. Negri, C. Bertarelli, C. Castiglioni, Biradicaloid character of thiophene-based heterophenoquinones: the role of electron–phonon coupling, Chemphyschem 11 (2010) 3685–3695.

[28] S. Di Motta, F. Negri, D. Fazzi, C. Castiglioni, E.V. Canesi, Biradicaloid and polyenic character of quinoidal oligothiophenes revealed by the presence of a low-lying double-exciton state, Journal of Physical Chemistry Letters 1 (2010) 3334–3339.

[29] R.S. Ashraf, M. Shahid, E. Klemm, M. Al-Ibrahim, S. Sensfuss, Thienopyrazine-based low-bandgap poly(heteroaryleneethynylene)s for photovoltaic devices, Macromolecular Rapid Communications 27 (2006) 1454–1459.

[30] W.Y. Wong, X.Z. Wang, Z. He, A.B. Djurisic, C.T. Yip, K.Y. Cheung, H. Wang, C.S.K. Mak, W.K. Chan, Metallated conjugated polymers as a new avenue towards high-efficiency polymer solar cells, Nature Materials 6 (2007) 521–527.

[31] S. Trasatti, The absolute electrode potential – an explanatory note (Recommendations 1986), Pure Applied Chemistry 58 (1986) 955–966.

[32] A. Tacca, R. Po, M. Caldararo, S. Chiaberge, L. Gila, L. Longo, P.R. Mussini, A. Pellegrino, N. Perin, M. Salvalaggio, A. Savoini, S. Spera, Ternary thiophene–X–thiophene semiconductor building blocks (X=fluorene, carbazole, phenothiazine): modulating electronic properties and electropolymerization ability by tuning the X core, Electrochimica Acta 56 (2011) 6638–6653.

[33] M.A. Faist, T. Kirchartz, W. Gong, R.S. Ashraf, I. McCulloch, J.C. de Mello, N.J. Ekins-Daukes, D.D.C. Bradley, J. Nelson, Competition between the charge transfer state and the singlet states of donor or acceptor limiting the efficiency in polymer:fullerene solar cells, Journal of the American Chemical Society 134 (2011) 685–692.

[34] Y. Suzuki, E. Miyazaki, K. Takimiya, ((Alkyloxy)carbonyl)cyanomethylene-substituted thienoquinoidal compounds: a new class of soluble n-channel organic semiconductors for air-stable organic field-effect transistors, Journal of the American Chemical Society 132 (2010) 10453–10466.

[35] T.J. Prosa, M.J. Winokur, J. Moulton, P. Smith, A.J. Heegerm, X-ray structural studies of poly(3-alkylthiophenes): an example of an inverse comb, Macromolecules 25 (1992) 4364–4372.

[36] A. Zen, M. Saphiannikova, D. Neher, J. Grenzer, S. Grigorian, U. Pietsch, U. Asawapirom, S. Janietz, U. Scherf, I. Lieberwirth, G. Wegner, Effect of molecular weight on the structure and crystallinity of poly(3-hexylthiophene), Macromolecules 39 (2006) 2162.

[37] T. Agostinelli, S. Lilliu, J.G. Labram, M. Campoy-Quiles, M. Hampton, E. Pires, J. Rawle, O. Bikondoa, D.D.C. Bradley, T.D. Anthopoulos, J. Nelson, J.E. Macdonald, Real-time investigation of crystallization and phase-segregation dynamics in P3HT:PCBM solar cells during thermal annealing, Advanced Materials 21 (2011) 1701–1708.

[38] J. Kirkpatrick, P.E. Keivanidis, A. Bruno, F. Ma, S.A. Haque, Y. Yarstev, V. Sundstrom, J. Nelson, Ultrafast transient optical studies of charge pair generation and recombination in poly-3-hexylthiophene(P3ht):[6,6]phenyl C61 butyric methyl acid ester (PCBM) blend films, Journal of Physical Chemistry B 115 (2011) 15174–15180.

[39] S. Yamamoto, J. Guo, H. Ohkita, S. Ito, Formation of methanofullerene cation in bulk heterojunction polymer solar cells studied by transient absorption spectroscopy, Advanced Functional Materials 18 (2008) 2555–2562.

[40] E.V. Canesi, G. Dassa, C. Botta, A. Bianco, C. Bertarelli, G. Zerbi, Optical features of substituted phenyl end-capped oligothiophenes, Open Chemical Physics Journal 1 (2008) 23–28.

[41] F. Machui, S. Rathgeber, N. Li, T. Ameri, C.J. Brabec, Influence of a ternary donor material on the morphology of a P3HT:PCBM blend for organic photovoltaic devices, Journal of Materials Chemistry 22 (2012) 15570–15577.

[42] E.P. Keivanidis, T.M. Clarke, S. Lilliu, T. Agostinelli, J.E. Macdonald, J.R. Durrant, D.D.C. Bradley, J. Nelson, Dependence of charge separation efficiency on film microstructure in Poly(3-hexylthiophene-2,5-diyl): [6,6]-Phenyl-C61 butyric acid methyl ester blend films, Journal of Physical Chemistry Letters 1 (2010) 734–738.

[43] S. Cook, H. Ohkita, Y. Kim, J.J. Benson-Smith, D.D.C. Bradley, J.R. Durrant, A photophysical study of PCBM thin films, Chemical Physics Letters 445 (2007) 276–280.

[44] Y.J. Cho, J.Y. Lee, B.D. Chin, F.S.R., Polymer bulk heterojunction photovoltaics employing a squaraine donor additive, Organic Electronics 14 (2013) 1081–1085.